

Electromechanical coupling effect in a ferroelectric *h*-PbO monolayer

Shuoke Xu, Xikui Ma,^{*} Kehan Liu, and Mingwen Zhao^{✉†}

School of Physics, Shandong University, Jinan 250100, China



(Received 10 August 2023; revised 20 December 2023; accepted 26 February 2024; published 15 March 2024)

The electromechanical coupling effect holds great promise in various applications, such as actuators and artificial muscles. In this study, using first-principles calculations, we demonstrate this effect in a two-dimensional (2D) buckled honeycomb configuration of lead oxide (*h*-PbO). The *h*-PbO monolayer exhibits robust 2D ferroelectric polarization of about 28 pC/m along the out-of-plane direction, owing to the buckled configuration, which lifts the mirror symmetry. The direction of electric polarization can be reversed by overcoming a moderate energy barrier of about 240 meV/unit cell, and the Curie temperature is evaluated to be up to 440 K. Interestingly, the distinct hybridization of O and Pb atoms leads to self-bending of the *h*-PbO monolayer with an optimal curvature ($1/R$) of about 0.46 \AA^{-1} , exhibiting strong coupling with the electric polarization. As the direction of electric polarization is reversed, the bending of the *h*-PbO monolayer will also be reversed. With the increase of the curvature, the energy required to reverse the electric polarization direction decreases. The electrobending effect in this *h*-PbO monolayer renders a promising strategy to regulate the mechanical and electronic properties and the interplay between them and thereby concepts for nanoscale actuator devices.

DOI: [10.1103/PhysRevApplied.21.034028](https://doi.org/10.1103/PhysRevApplied.21.034028)

I. INTRODUCTION

The electrobending effect utilizes an electric field to induce bending or deformation in specific materials, such as dielectric elastomers or electroactive polymers [1–3]. These materials exhibit remarkable deformability in response to the electric field, resulting in significant changes to their shape. This electromechanical coupling effect enables precise control over the material's behavior, making it an invaluable component for designing adaptable and flexible systems. By applying an electric field, engineers and researchers can achieve controlled and reversible motion and actuation, facilitating a wide range of applications, including actuators and artificial muscles [4,5], across various fields. To expand their usability in demanding environments, such as aerospace, automotive, and industrial settings, where high-temperature conditions prevail, it is imperative to enhance the thermal stability of these materials.

The emergence of nanomaterials offers a promising platform for the development of nanoactuators [6,7], which are devices capable of precise mechanical motion at the nanoscale. Nanoactuators play a crucial role in various fields, including nanotechnology, microelectromechanical systems, robotics, medicine, and electronics. The bending behavior of two-dimensional (2D) materials in response

to an electric field enables nanoscale manipulation and engineering, making them highly promising for building nanoactuators [7–9]. Of particular interest among 2D materials are ferroelectric (FE) 2D materials with spontaneous ferroelectric polarization below the Curie temperature. The reversible ferroelectric polarization of these materials, especially those with out-of-plane electronic polarization, provides an additional means to control the shape of the 2D materials by applying an electric field. To date, several 2D out-of-plane ferroelectric materials have been theoretically predicted or experimentally demonstrated, including group-IV monochalcogenide monolayers, Sc_2CO_2 , $\text{Hf}_2\text{VC}_2\text{F}_2$, CuInP_2S_6 , $\alpha\text{-In}_2\text{Se}_3$, and more [10–17]. Notably, some of these 2D ferroelectric materials exhibit high Curie temperatures above room temperature [13–17]. However, none of them have been reported to possess the electrobending effect required to manipulate the shape of 2D materials by applying an electric field. Exploring 2D ferroelectric materials with electrobending capabilities holds great promise for advancing nanoscale actuation and engineering of nanodevices. The ability to precisely control the shape of 2D materials using an electric field could lead to innovative applications in nanoscale technologies and beyond.

Here, we present compelling evidence, derived from first-principles calculations, that showcases the remarkable electromechanical coupling effect in a 2D buckled honeycomb configuration of lead oxide (*h*-PbO) with out-of-plane ferroelectric polarization. The reversal of the electric

*mxk2022@sdu.edu.cn

✉zwm@sdu.edu.cn

polarization direction requires a moderate energy barrier of approximately 240 meV/unit cell to be overcome, while the Curie temperature reaches an impressive 440 K. A key finding is the distinct hybridization of O and Pb atoms, which triggers spontaneous bending in the *h*-PbO monolayer. We observe an optimal curvature ($\kappa \equiv 1/R$) of about 0.46 \AA^{-1} , leading to a fascinating bidirectional relationship: when the direction of electric polarization is reversed, the bending of the *h*-PbO monolayer also reverses accordingly, demonstrating a strong electromechanical coupling effect. Additionally, the bending of the monolayer can reciprocally alter the direction of the out-of-plane ferroelectric polarization once the curvature surpasses a critical value. These intriguing results shed light on the complex interplay between bending and electric polarization in *h*-PbO monolayers, holding great promise for responsive nanodevices, particularly nanoactuators. The electromechanical coupling effect offers a pivotal means to tailor the properties of such nanodevices for specific functionalities, making *h*-PbO monolayers a highly attractive material for various potential applications.

II. METHODS AND COMPUTATIONAL DETAILS

We conducted first-principles calculations based on density-functional theory (DFT) using the Vienna *ab initio* simulation package [18,19]. The interactions between ions and valence electrons were treated with the projector-augmented-wave method [20,21]. For the exchange-correlation functional, we employed the generalized gradient approximation with the Perdew, Burke, and Ernzerhof formula in the structural optimization and electronic property analysis [22], while the Heyd-Scuseria-Ernzerhof (HSE06) hybrid functional was adopted in the electronic-band-structure calculations [23]. The energy cutoff for the plane-wave basis was 520 eV and a Γ -centered k -point mesh of $18 \times 18 \times 1$ was applied in sampling the Brillouin zone. The convergence threshold parameters were set to be 10^{-5} and 10^{-2} eV \AA , for the total energies and the forces, respectively. A vacuum space of 25 \AA was involved in the z direction to prevent mutual interaction between adjacent images.

For investigating bending deformation, nanotubes with different diameters were employed to explore various bending curvatures. A vacuum space of 50 \AA was applied to minimize the interactions between neighboring nanotubes, and the Brillouin zone was sampled with $1 \times 1 \times 10 k$ points. The coordinates and the lattice vectors of the structures have been meticulously optimized to accommodate the surface relaxation of the systems. The ferroelectric polarization was determined using the Berry phase method, while the energy barrier between two FE states was computed using the climbing-image nudged elastic band (CI NEB) method [24,25]. Additionally,

we calculated the phonon spectra using the PHONOPY code [26].

III. RESULTS AND DISCUSSION

A. Strategy for electromechanical coupling in ferroelectric 2D materials

We begin with a 2D material featuring a fascinating combination of out-of-plane electric polarization and intrinsic bending configuration, as depicted in Fig. 1(a). The bending in this electrically polarized 2D material arises from the distinct binding nature of its atoms in the two sublayers, with opposite charges and distinct orbital hybridization preferences. As a result, when an external electric field is applied to reverse the electric polarization direction, the bending direction is also simultaneously revised, showcasing a strong electromechanical coupling effect. Conversely, when the bending direction of the 2D ferroelectric material is reversed, the electric polarization direction follows suit accordingly. This bidirectional relationship enables precise control over the shape of the 2D ferroelectric material through the application of an electric field, and the bending vibration of the material can be activated through resonance with an alternating electric field. Furthermore, in a 2D ferroelectric material containing multiple domains with opposite electric polarization, the motion of domain walls can be induced by an external electric field, resulting in undulating movement within the material. These distinctive scenarios, driven by the electromechanical coupling effect, hold exceptional promise in the development of nanoactuators. These nanoactuators could find applications in a wide range of fields due to their

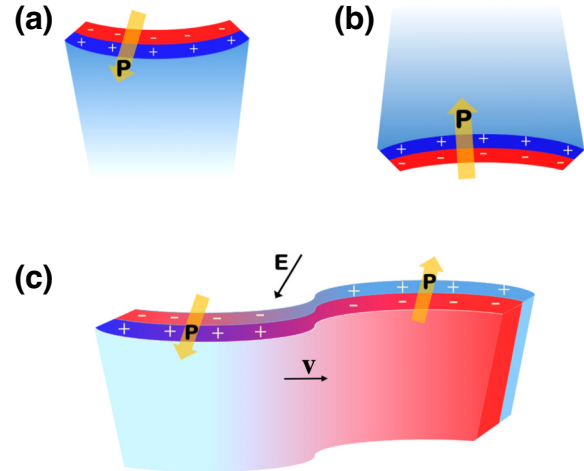


FIG. 1. Schematic representation of tunable self-bending scenario of a 2D ferroelectric materials with out-of-plane polarization. (a),(b) Bending of a 2D ferroelectric material in response to reverse electric polarization. (c) Motion of a domain wall between two ferroelectric states with opposite polarization directions subjected to an external electric field.

ability to respond to and manipulate electric fields, offering exciting possibilities for advanced nanotechnology and responsive devices.

B. Material design of ferroelectric *h*-XY monolayers

To realize the aforementioned scenarios, 2D ferroelectric materials must meet specific criteria: (1) they should exhibit stable ferroelectric polarization along the out-of-plane direction; (2) the energy barrier for reversing the electric polarization direction should be both low enough for practical experimental manipulation and large enough to maintain polarization stability at high temperatures; and (3) these materials need to possess an inherent bending tendency with a substantial optimal curvature, where the direction of bending relies on the orientation of electric polarization.

Based on the aforementioned criteria, we evaluated the potential of XY monolayers (where $X = \text{Si, Ge, Sn, Pb}$ and $Y = \text{O, S, Se, Te}$) with a buckled honeycomb lattice (*h*-XY) as promising electrobending materials. Their stability and feasibility have been previously verified [10]. In these *h*-XY monolayers, the X and Y atoms, possessing distinct electronegativities, occupy different sublattices of the buckled honeycomb lattice, leading to a notable electric polarization along the out-of-plane direction. The out-of-plane electric polarization in the *h*-XY monolayers is reminiscent of that observed in Janus materials, where the in-plane mirror symmetry is absent [27]. It is noteworthy that specific binary honeycomb lattices, like BN, AlN, and SiC monolayers [28–30], demonstrate a preference for planar configurations without any out-of-plane electric polarization. This characteristic is associated with the distinct orbital hybridization of their constituent atoms. In these planar configurations, both C and N atoms exhibit a preference for sp^2 hybridization, similar to the configuration observed in graphene. In contrast, the atoms in *h*-XY monolayers exhibit a preference for sp^3 -like hybridization, akin to silicene [31], leading to buckling configurations and the subsequent emergence of out-of-plane electric polarization [10]. The distinction in orbital hybridization underpins the difference in energetically preferable configurations between the two types of honeycomb lattices.

Another compelling reason for selecting *h*-XY monolayers is their unique property of reversible electric polarization direction by simply reversing the buckling direction of the monolayers. Notably, the planar configuration without out-of-plane polarization (PE) serves as the transition state between the two ferroelectric states (FE and FE'). The energy barrier between two ferroelectric states has been widely employed for evaluating the feasibility of reversing the electric polarization direction, as well as the stability and robustness of electric polarization [32,33]. To quantify the energy barrier required for reversing the electric polarization direction in *h*-XY monolayers, we employed

the CI NEB method. Figure 2(b) displays the energy-barrier analysis, revealing that, among the *h*-XY monolayers examined, the *h*-PbO monolayer exhibits the lowest energy barrier, measuring approximately 240 meV/unit cell. Remarkably, this energy-barrier magnitude is comparable to that (320 meV/unit cell) observed in the 2D ferroelectric CuCrS₂ material with out-of-plane electric polarization [34], signifying its feasibility and practical operability in experimental settings. Notably, the PbO monolayer also has other allotropes besides *h*-PbO, such as α -PbO [35], β -PbO [36], FE-PbO [37], and δ -PbO [38]. Our calculations show that the *h*-PbO monolayer is less energetically stable than these allotropes by about 0.63, 0.62, 0.62, and 0.56 eV/atom, respectively, implying the metastability of the *h*-PbO monolayer, which is consistent with results reported previously in the literature [10]. The dynamic stability of the *h*-PbO monolayer has been verified through the phonon-spectrum calculations, where no imaginary modes were observed, as shown in Fig. 2(d). Given its favorable characteristics, we direct our focus towards investigating the *h*-PbO monolayer in subsequent sections to delve deeper into its potential and applications in the context of the electrobending effect.

C. Electric properties of the ferroelectric *h*-PbO monolayer

The presence of ferroelectricity in the *h*-PbO monolayer is further corroborated by the double-wall energy profile, as depicted in Fig. 2(c). To quantify the spontaneous polarization of the *h*-PbO monolayer, we utilized the Berry phase method [39]; this is currently the most widely adopted approach for calculating the electric polarization of semiconductors, as demonstrated in numerous studies [40,41]. Our calculations reveal that the *h*-PbO monolayer exhibits an electric polarization of approximately $P = 28$ pC/m. Notably, this magnitude is significantly higher, by 1–2 orders of magnitude, than those observed in other 2D honeycomb binary compounds, such as SiGe and InP monolayers [42,43]. We ascribed this higher polarization to the pronounced buckling effect ($h = 0.92$ Å) and the substantial difference in electronegativity between O and Pb atoms. This large electric polarization is expected to significantly enhance the electrobending effect of the *h*-PbO monolayer, making it an attractive candidate for various applications. Furthermore, phonon-spectrum analysis, as illustrated in Fig. 2(d), confirms the material's stability, reinforcing its suitability for experimental exploration and practical implementation in potential nanodevice applications.

Figure 3(a) illustrates the electronic band structure of the *h*-PbO monolayer, which is acquired through precise DFT calculations utilizing the HSE06 functional for increased accuracy. The analysis reveals that the *h*-PbO monolayer possesses an indirect band gap with a magnitude of

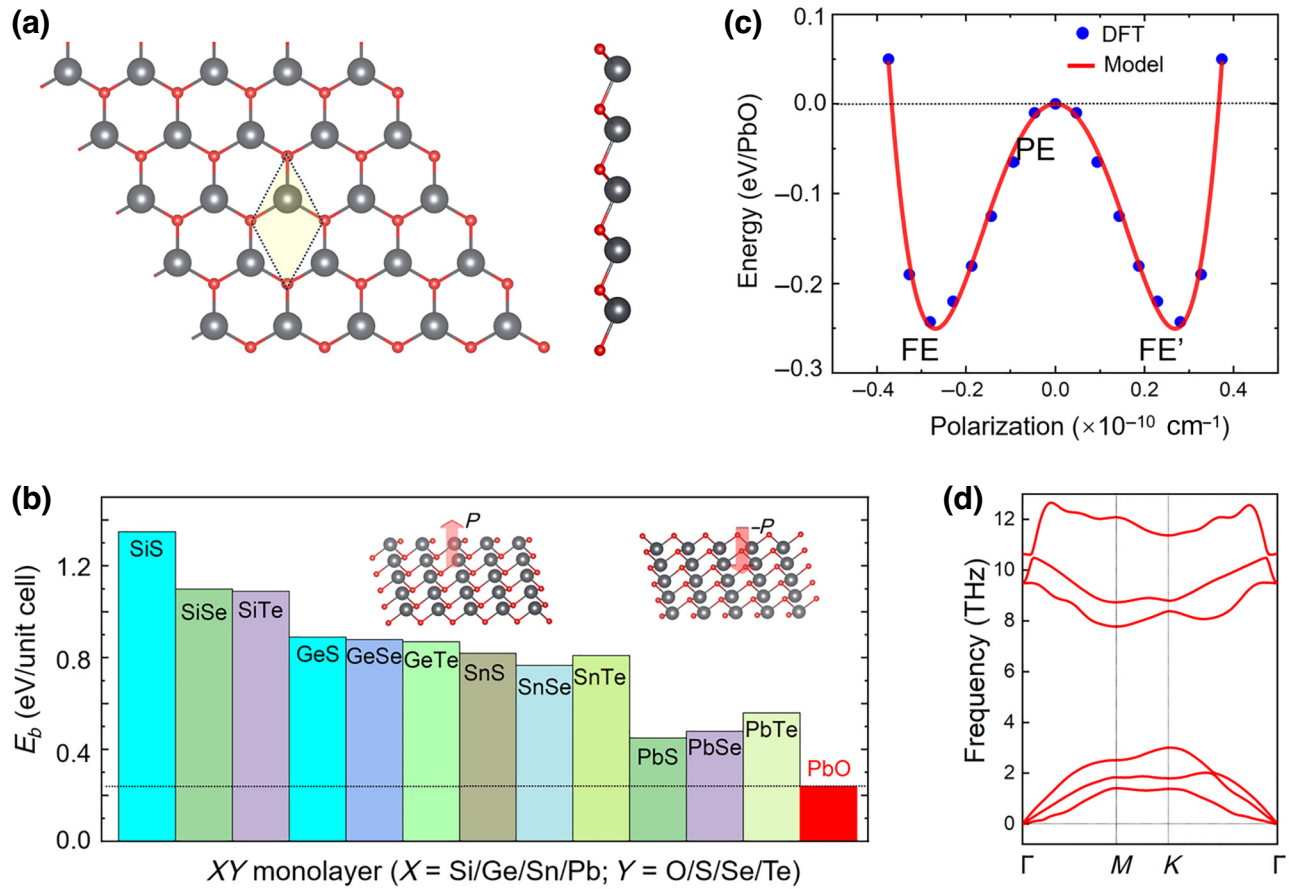


FIG. 2. Candidate 2D ferroelectric materials with electrobending effect. (a) Buckled honeycomb lattice of XY monolayers ($X = \text{Si}, \text{Ge}, \text{Pb}; Y = \text{O}, \text{S}, \text{Se}, \text{Te}$). Primitive cell is indicated by the rhombus. (b) Energy barriers of the XY monolayers required to reverse the electric polarization direction. (c) Energy profiles of the $h\text{-PbO}$ monolayer obtained from DFT calculations (dots) and fitting data (red line), according to the Landau-Ginzburg phase transition theory. (d) Phonon spectrum of $h\text{-PbO}$ monolayer without bending.

2.60 eV. Specifically, the valence-band maximum (VBM) is located at the K point, while the conduction-band minimum (CBM) is situated at the Γ point in the Brillouin zone. Upon further investigation, it becomes evident that the states contributing to the VBM primarily arise from the p_z orbitals of O atoms, while the states responsible for the CBM mainly originate from the p_z orbitals of Pb atoms. This understanding of the orbital contributions aids in comprehending the electronic structure and the mechanisms governing charge transfer and band-gap characteristics in the $h\text{-PbO}$ monolayer, offering valuable insights for potential electronic applications.

According to the Landau-Ginzburg phase-transition theory, the polarization-dependent energies of the $h\text{-PbO}$ monolayer obtained from the DFT calculations can be fitted using the following expression [44,45]:

$$E(P) = \sum_i \left(\frac{A}{2} P_i^2 + \frac{B}{4} P_i^4 + \frac{C}{6} P_i^6 \right) + \frac{D}{2} \sum_{\langle i,j \rangle} (P_i - P_j)^2. \quad (1)$$

This expression can be regarded as the Taylor series of local structural distortions with a specific polarization defined at each unit cell, P_i . The parameters A , B , and C correspond to the anharmonic double-well potentials associated with the energy contribution from local modes of the second, fourth, and sixth order, respectively. The second term in the expression denotes the coupling between the nearest local electric dipoles (Ginzburg term), and the parameter D describes the average dipole-dipole interaction. These parameters can be acquired through fitting the data from DFT calculations, utilizing the mean-field theory within the nearest-neighbor approximation. In the DFT calculations, we utilized large-size supercells characterized by distinct electric polarization orderings to obtain polarization-dependent energies for subsequent fitting processes. The parameters have been fitted to the following values: $A = -110.54 \times 10^2$ meV, $B = 9.47 \times 10^4$ meV, $C = 0.48 \times 10^6$ meV, and $D = 2.96 \times 10^2$ meV, with the fitted data represented by the red line in Fig. 2(c).

Utilizing the effective Hamiltonian constructed using Eq. (1) and the aforementioned parameters, we conducted

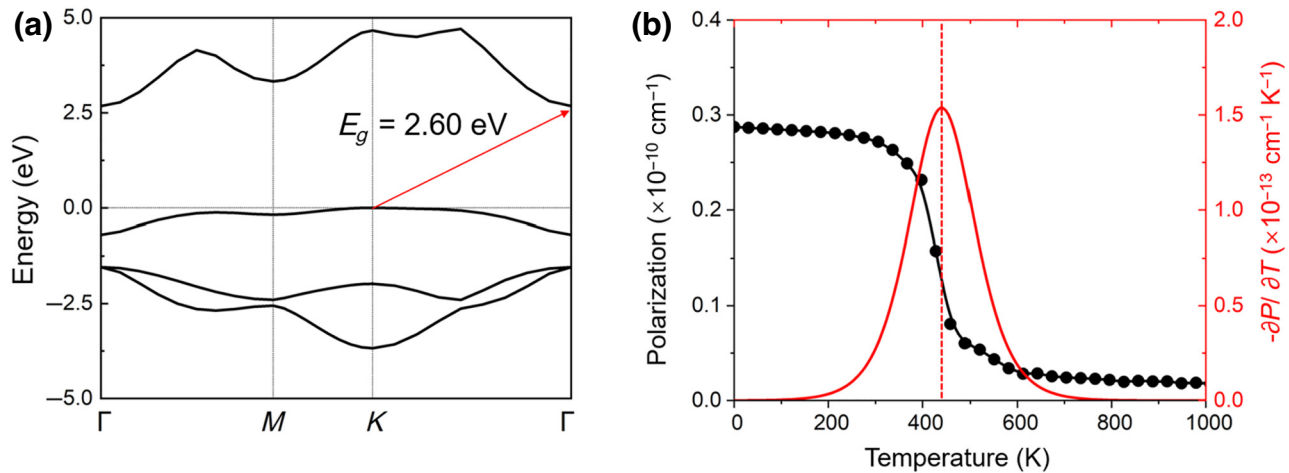


FIG. 3. Electronic band structure and electric polarization properties of the *h*-PbO monolayer. (a) Electronic band structure of the *h*-PbO monolayer obtained from DFT + HSE06 calculations. Energy of the valence-band maximum is set to zero. Indirect band gap is indicated by the red arrow. (b) Variation of electric polarization, P (black dots and line), and $-\partial P/\partial T$ (red line) as a function of temperature.

Monte Carlo (MC) simulations to investigate the phase transition of the *h*-PbO monolayer. The electric polarization (P) of the *h*-PbO monolayer at different temperatures obtained from MC simulations is depicted in Fig. 3(b). We observed an abrupt transition at $T_c \approx 440$ K. Furthermore, we calculated the pyroelectric coefficient, $-\partial P/\partial T$, where its peak corresponds to the Curie temperature. The red line in Fig. 3(b) shows the peak value, and based on our calculations, the Curie temperature of the *h*-PbO monolayer is approximately 440 K, indicating its stability at high temperatures.

D. Electromechanical coupling in the ferroelectric *h*-PbO monolayer

To investigate the bending effect of the *h*-PbO monolayer, we constructed *h*-PbO nanotubes by rolling a *h*-PbO sheet along the zigzag direction. Two distinct nanotube configurations were considered: (1) where oxygen (lead) atoms reside in the interior (exterior) wall of the nanotubes, respectively, as shown in Fig. 4(a); (2) where oxygen (lead) atoms reside in the exterior (interior) wall of the nanotubes, respectively, as shown in Fig. 4(b). The radius of the nanotubes (R) was defined as the average value of the radii of the O and Pb cylinders, and the curvature of the nanotubes was represented as the inverse of the radius, $1/R$. For clarity, we denoted the nanotubes with Pb atoms on the exterior surface as $R > 0$ and those with O atoms on the exterior surface as $R < 0$, as illustrated in Figs. 4(a) and 4(b).

The energy profiles of the *h*-PbO nanotubes with different curvatures are plotted in Fig. 4(c), setting the energy of the unbent *h*-PbO monolayer ($1/R = 0$) to zero. The figure revealed the following observations. (1) The *h*-PbO nanotubes with O atoms on the exterior surface ($R < 0$)

were energetically unfavorable compared to the unbent *h*-PbO monolayer, suggesting that this bending configuration is energetically disadvantageous. (2) Conversely, the *h*-PbO nanotubes with Pb atoms on the exterior surface ($R > 0$) exhibited greater energy favorability than the unbent *h*-PbO monolayer, indicating the feasibility of a self-bending scenario for the *h*-PbO monolayer. (3) The curvature-dependent energies of the *h*-PbO nanotubes can be fitted using the following expression:

$$E(R^{-1}) = C_1 R^{-1} + C_2 R^{-2} + C_3 R^{-3} + C_4 R^{-4}. \quad (2)$$

This expression can be regarded as the Taylor series of local curvature (R^{-1}) [43]. The fitting parameters are $C_1 = -1.896 \text{ eV } \text{\AA}$, $C_2 = 3.916 \text{ eV } \text{\AA}^2$, $C_3 = -10.383 \text{ eV } \text{\AA}^3$, and $C_4 = 11.944 \text{ eV } \text{\AA}^4$, as represented by the blue line in Fig. 4(c). The fitting yielded a local energy minimum at a radius of $R = 2.17 \text{ \AA}$. This small optimal radius (large curvature) implies a strong self-bending effect of the *h*-PbO monolayer.

The self-bending phenomenon observed in the *h*-PbO monolayer can be attributed to the distinct binding characteristics of its constituent O and Pb atoms. Despite both Pb and O atoms in the *h*-PbO monolayer preferring sp^3 hybridization, the resulting bond angles of Pb-O-Pb (α) and O-Pb-O (β) deviate from the standard value of sp^3 hybridization (109.5°) to different extents. In the energetically most favorable *h*-PbO nanotube, these bond angles were determined to be $\alpha = 124.6^\circ$ (100.1°) and $\beta = 89.8^\circ$ (84.8°). It is evident that O atoms prefer a bond angle larger than 109.5° , while Pb atoms favor a bond angle smaller than 109.5° . This difference in preferred bond angles drives the self-bending scenario of the *h*-PbO monolayer, with O atoms positioned on the interior surface. As a result, the

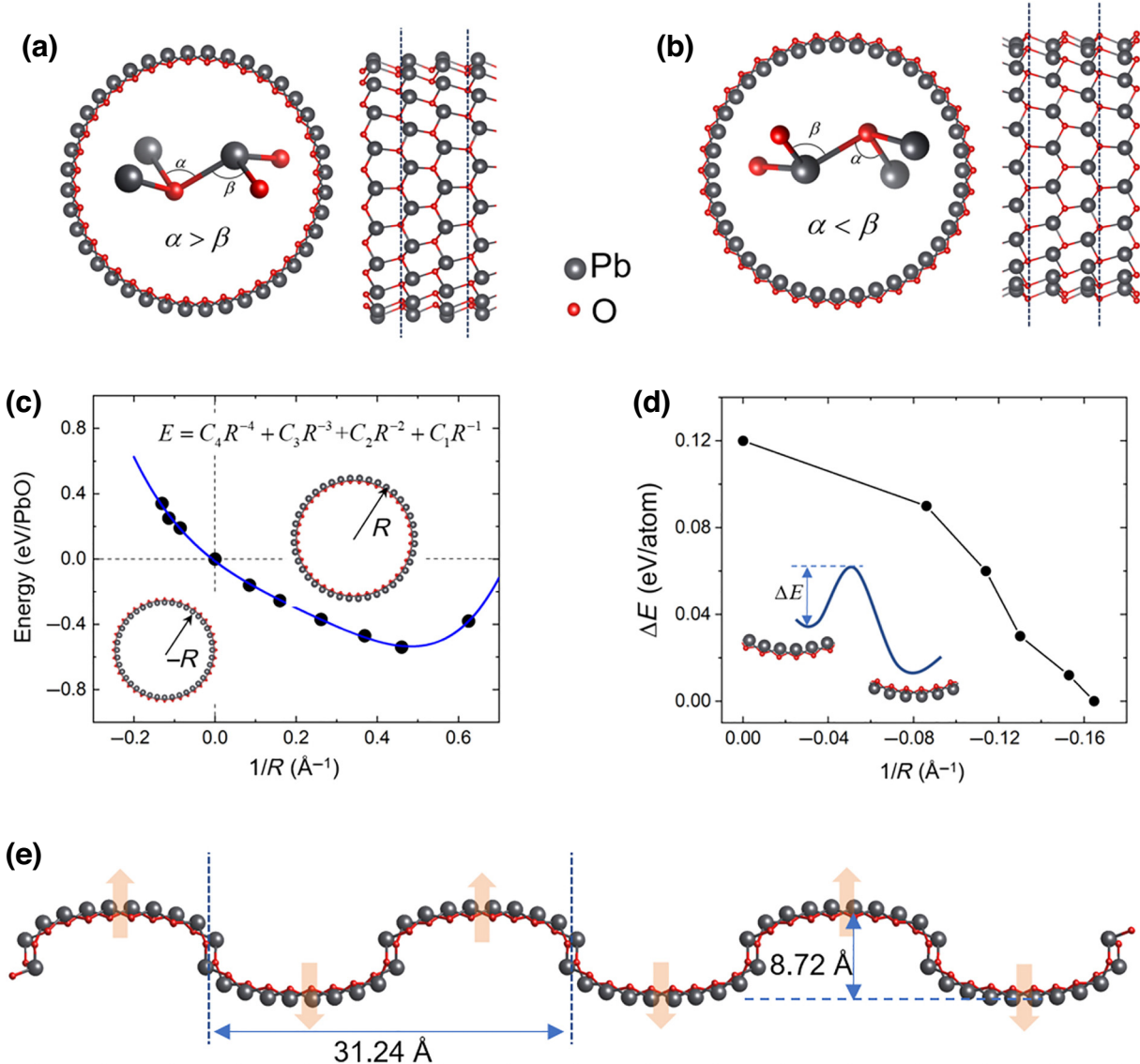


FIG. 4. Electrobending effect of *h*-PbO monolayer. (a),(b) *h*-PbO nanotube models for evaluating the intrinsic bending of *h*-PbO monolayer. Local atomic configurations of these nanotubes are plotted in the insets. (c) Energies of *h*-PbO nanotubes with different curvatures. Blue line indicates data fitted using the expression $E = C_4R^{-4} + C_3R^{-3} + C_2R^{-2} + C_1R^{-1}$, with $C_4 = 11.944 \text{ eV \AA}^4$ and $C_3 = -10.383 \text{ eV \AA}^3$, $C_2 = 3.92 \text{ eV \AA}^2$, and $C_1 = -1.85 \text{ eV \AA}$. (d) Energy barriers required to reverse the electric polarization of *h*-PbO monolayer with different curvatures. (e) Atomic configuration of a *h*-PbO monolayer containing multidomains. Dashed lines indicate the size of the supercell.

monolayer exhibits a curved or bent configuration. From this observation, we can infer that whether a 2D buckled honeycomb binary compound favors a self-bending scenario is closely related to the disparity in the preferred binding orientations between its constituent atoms. The distinct bond-angle preferences of the atoms play a crucial role in determining the structural characteristics and bending behavior of such materials. Understanding these binding characteristics can guide the design and engineering of 2D materials with tailored properties for specific applications.

The considerable energetic advantage of *h*-PbO nanotubes with O atoms on the interior surface suggests a promising approach to control the bending of the *h*-PbO monolayer by manipulating the electric polarization direction. Specifically, reversing the electric polarization of a self-bent *h*-PbO monolayer can be achieved by applying an external electric field in the opposite direction of its inherent polarization, thereby reversing the bending direction of the *h*-PbO monolayer as well. Conversely, if the bending direction of a self-bent *h*-PbO monolayer is altered (e.g., through the application of external tensile

strain), the electric polarization direction may also reverse accordingly.

To explore the feasibility of this strategy, we conducted calculations to determine the energy barriers associated with reversing the electric polarization direction in the bent *h*-PbO monolayer. As depicted in Fig. 4(d), the energy barrier diminishes with an increase in bending curvature and vanishes when the bending curvature reaches $1/R = -0.16 \text{ \AA}^{-1}$. This suggests that the response of the electric polarization direction to the bending of the *h*-PbO monolayer becomes nearly barrierless beyond this critical curvature value. The high energetic preferability of the bent *h*-PbO monolayer with O atoms on the interior wall, in contrast to that with O atoms on the exterior wall, accounts for this phenomenon. As the curvature increases, the energy of the bent *h*-PbO monolayer with O atoms on the exterior wall rises, as indicated in Fig. 4(c), eventually surpassing that of the transition state as the curvature exceeds the critical value. Consequently, the reversal of the electric polarization direction becomes barrierless. This suggests that the reversal of the electric polarization direction would initiate in the regions characterized by significant local curvature. Overall, due to the pronounced energetic advantage of *h*-PbO nanotubes with O atoms on the interior surface, it is feasible to control the bending and electric polarization direction of the *h*-PbO monolayer by external means, making it a promising avenue for potential applications.

We have examined the variation of the surface buckling (*h*), defined as the nearest distance between Pb and O atoms along the radial direction, which dictates the magnitude of local electric dipole moments, with respect to the bending curvature. Our calculations demonstrate a gradual decrease in surface buckling as the curvature ($1/R$) increases. Specifically, for the PbO nanotube with a curvature of 0.46 \AA^{-1} , the surface buckling reduces to 0.52 \AA , compared to the value of 0.92 \AA observed for the *h*-PbO monolayer. Notably, the charges of Pb and O exhibit insensitivity to the bending curvature. Consequently, we deduce that the local electric polarization diminishes with the increase in bending curvature.

Remarkably, the self-bending phenomenon has been documented in other two-dimensional materials characterized by out-of-plane electric polarization, such as aluminosilicate [46,47], As-graphene [48], and diamondene [49]. However, it is worth noting that, in these materials, the direction of both electric polarization and bending remains unalterable through external electric fields, thereby precluding their utilization in achieving the electromechanical coupling effect, as discussed earlier. We also examined the potential self-bending phenomenon in other *h*-XY monolayers. In contrast to the case of the *h*-PbO monolayer, our calculations demonstrated that the planar configurations of these *h*-XY monolayers were stabilized by the emergence of an energy barrier between

the planar configuration and the self-bending state. We attribute this difference to the remarkable out-of-plane buckling observed in these *h*-XY monolayers compared to the *h*-PbO monolayer. The self-bending scenario observed in the *h*-PbO monolayer arises from its unique bonding characteristics, which delicately balance the buckling strength and surface structural reconstruction.

We also explored the self-bending scenario of the *h*-PbO monolayer by employing armchair nanotube models. Our investigation revealed that the armchair *h*-PbO nanotube exhibits an energetic unfavorability compared to a zigzag nanotube of similar radius. Specifically, the most energetically favorable armchair nanotube is less stable than its zigzag counterpart by approximately 0.09 eV per PbO unit. Consequently, the *h*-PbO monolayer demonstrates a preference for self-bending along the zigzag direction rather than the armchair direction.

Lastly, we explore a wavelike configuration of the *h*-PbO monolayer, comprising two electric polarization domains arranged periodically, as illustrated in Fig. 4(e). We considered three supercells containing 40, 48, and 56 atoms, respectively. Structural optimization consistently reveals the presence of walls between the two domains, which are characterized by periodicities of 31.24, 37.56, and 43.97 \AA , respectively. Remarkably, these wave-like configurations prove to be energetically more favorable than the unbent *h*-PbO monolayer by approximately 0.32, 0.20, and 0.17 eV per PbO unit. These findings strongly support the feasibility of forming multidomains in the *h*-PbO monolayer. The observed increase in energy with the augmentation of periodicity is attributed to the reduction in local bending curvature. Notably, the domain walls display a distinct configuration, spanning just a few atomic arrays. The presence of such multidomain structures opens up intriguing possibilities for tailoring the properties of the *h*-PbO monolayer and could have significant implications for potential applications in nanoelectronics and other related fields. Further investigations into the properties and behaviors of these multidomain structures will likely yield valuable insights into their potential use in various devices and materials.

IV. CONCLUSION

Our study presents a highly promising strategy for achieving electric-mechanical coupling in 2D materials through the electrobending effect. Utilizing first-principles calculations, we demonstrate that the *h*-PbO monolayer with a buckled honeycomb configuration exhibits robust ferroelectric polarization along the out-of-plane direction, coupled with a self-bending phenomenon originating from the distinct orbital hybridization of O and Pb atoms. The electric polarization direction can be reversed with a moderate energy barrier of approximately 240 meV/unit cell, and the Curie temperature is found to reach up to 440 K.

Moreover, the reversal of electric polarization directly impacts the bending behavior of the *h*-PbO monolayer, further showcasing the strong interplay between electrical and mechanical properties. Notably, we observe that the energy required to switch the direction of electric polarization decreases as the curvature increases. This unique electrobending effect in the *h*-PbO monolayer holds great promise in regulating both the mechanical and electronic properties, opening up exciting possibilities for nanoscale actuator devices. Furthermore, other buckled honeycomb lattices formed by binary compounds could potentially provide a promising avenue for achieving this electromechanical coupling effect, aligning with the three criteria proposed in this study.

ACKNOWLEDGMENTS

This study is supported by the National Natural Science Foundation of China (Grant No. 21833004) and the Taishan Scholar Foundation of Shandong Province.

- with high transition temperature, *J. Am. Chem. Soc.* **140**, 9768 (2018).
- [13] F. Liu, L. You, K. L. Seyler, X. Li, P. Yu, J. Lin, X. Wang, J. Zhou, H. Wang, H. He, S. T. Pantelides, W. Zhou, P. Sharma, X. Xu, P. M. Ajayan, J. Wang, and Z. Liu, Room-temperature ferroelectricity in CuInP₂S₆ ultrathin flakes, *Nat. Commun.* **7**, 12357 (2016).
 - [14] Y. Zhou, D. Wu, Y. Zhu, Y. Cho, Q. He, X. Yang, K. Herrera, Z. Chu, Y. Han, M. C. Downer, H. Peng, and K. Lai, Out-of-plane piezoelectricity and ferroelectricity in layered α -In₂Se₃ nanoflakes, *Nano Lett.* **17**, 5508 (2017).
 - [15] C. Cui, W. Hu, X. Yan, C. Addieg, W. Gao, Y. Wang, Z. Wang, L. Li, Y. Cheng, P. Li, X. Zhang, H. N. Alshareef, T. Wu, W. Zhu, X. Pan, and L. Li, Intercorrelated in-plane and out-of-plane ferroelectricity in ultrathin two-dimensional layered semiconductor In₂Se₃, *Nano Lett.* **18**, 1253 (2018).
 - [16] K. Chang, J. Liu, H. Lin, N. Wang, K. Zhao, A. Zhang, F. Jin, Y. Zhong, X. Hu, W. Duan, Q. Zhang, L. Fu, Q. Xue, X. Chen, and S. Ji, Discovery of robust in-plane ferroelectricity in atomic-thick SnTe, *Science* **353**, 274 (2016).
 - [17] C. Zheng, L. Yu, L. Zhu, J. L. Collins, D. Kim, Y. Lou, C. Xu, M. Li, Z. Wei, Y. Zhang, M. T. Edmonds, S. Li, J. Seidel, Y. Zhu, J. Z. Liu, W. Tang, and M. S. Fuhrer, Room temperature in-plane ferroelectricity in van der Waals In₂Se₃, *Sci. Adv.* **4**, eaar7720 (2018).
 - [18] G. Kresse and J. Hafner, *Ab initio* molecular dynamics for open-shell transition metals, *Phys. Rev. B* **48**, 13115 (1993).
 - [19] G. Kresse and J. Furthmüller, Efficiency of *ab-initio* total energy calculations for metals and semiconductors using a plane-wave basis set, *Comput. Mater. Sci.* **6**, 15 (1996).
 - [20] G. Kresse and D. Joubert, From ultrasoft pseudopotentials to the projector augmented-wave method, *Phys. Rev. B* **59**, 1758 (1999).
 - [21] P. E. Blöchl, Projector augmented-wave method, *Phys. Rev. B* **50**, 17953 (1994).
 - [22] J. P. Perdew, A. Ruzsinszky, G. I. Csonka, O. A. Vydrov, G. E. Scuseria, L. A. Constantin, X. Zhou, and K. Burke, Restoring the density-gradient expansion for exchange in solids and surfaces, *Phys. Rev. Lett.* **100**, 136406 (2008).
 - [23] J. Paier, M. Marsman, K. Hummer, G. Kresse, I. C. Gerber, and J. G. Ángyán, Screened hybrid density functionals applied to solids, *J. Chem. Phys.* **124**, 154709 (2006).
 - [24] R. D. King-Smith and D. Vanderbilt, Theory of polarization of crystalline solids, *Phys. Rev. B* **47**, 1651 (1993).
 - [25] G. Henkelman, B. P. Uberuaga, and H. Jónsson, A climbing image nudged elastic band method for finding saddle points and minimum energy paths, *J. Chem. Phys.* **113**, 9901 (2000).
 - [26] A. Togo and I. Tanaka, First principles phonon calculations in materials science, *Scr. Mater.* **108**, 1 (2015).
 - [27] A. Lu, H. Zhu, J. Xiao, C. Chuu, Y. Han, M. Chiu, C. Cheng, C. Yang, K. Wei, Y. Yang, Y. Wang, D. Sokaras, D. Nordlund, P. Yang, D. Muller, M. Y. Chou, X. Zhang, and L. Li, Janus monolayers of transition metal dichalcogenides, *Nat. Nanotechnol.* **12**, 744 (2017).
 - [28] A. Rubio, J. L. Corkill, and M. L. Cohen, Theory of graphitic boron nitride nanotubes, *Phys. Rev. B* **49**, 5081(R) (1994).

- [29] M. W. Zhao, Y. Y. Xia, D. J. Zhang, and L. M. Mei, Stability and electronic structure of AlN nanotubes, *Phys. Rev. B* **68**, 235415 (2003).
- [30] M. W. Zhao, Y. Y. Xia, F. Li, R. Q. Zhang, and S. T. Lee, Strain energy and electronic structures of silicon carbide nanotubes: Density functional calculations, *Phys. Rev. B* **71**, 085312 (2005).
- [31] S. Cahangirov, M. Topsakal, E. Aktürk, H. Sahin, and S. Ciraci, Two- and one-dimensional honeycomb structures of silicon and germanium, *Phys. Rev. Lett.* **102**, 236804 (2009).
- [32] L. Qi, S. C. Ruan, and Y. J. Zeng, Review on recent developments in 2D ferroelectrics: Theories and applications, *Adv. Mater.* **33**, 2005098 (2021).
- [33] Q. Yang, W. Xiong, L. Zhu, G. Y. Gao, and M. H. Wu, Chemically functionalized phosphorene: Two-dimensional multiferroics with vertical polarization and mobile magnetism, *J. Am. Chem. Soc.* **139**, 11506 (2017).
- [34] T. Zhong, X. Li, M. Wu, and J. Liu, Room-temperature multiferroicity and diversified magnetoelectric couplings in 2D materials, *Natl. Sci. Rev.* **7**, 373 (2020).
- [35] M. H. Zhang, X. L. Chen, W. X. Ji, P. J. Wang, M. Y. Yuan, and C. W. Zhang, Discovery of multiferroics with tunable magnetism in two-dimensional lead oxide, *App. Phys. Lett.* **116**, 172105 (2020).
- [36] Y. Liang, X. Lv, and Th. Frauenheim, Carrier doping-induced strong magnetoelastic coupling in 2D lattice, *Nanoscale* **14**, 3261 (2022).
- [37] Y. Jia, F. Luo, X. Hao, Q. Meng, W. Dou, L. Zhang, J. Wu, S. Zhai, and M. Zhou, Intrinsic valley polarization and high-temperature ferroelectricity in two-dimensional orthorhombic lead oxide, *ACS Appl. Mater. Interfaces* **13**, 6480 (2021).
- [38] S. Xu, X. Ma, Y. Li, Y. Qu, and M. Zhao, Two-dimensional multiferroic δ -PbO monolayer with a large in-plane negative Poisson's ratio, *ACS Appl. Electron. Mater.* **4**, 2264 (2022).
- [39] N. A. Spaldin, A beginner's guide to the modern theory of polarization, *J. Solid State Chem.* **195**, 2 (2012).
- [40] C. X. Huang, Y. P. Du, H. P. Wu, H. J. Xiang, K. M. Deng, and E. J. Kan, Prediction of intrinsic ferromagnetic ferroelectricity in a transition-metal halide monolayer, *Phys. Rev. Lett.* **120**, 147601 (2018).
- [41] Y. Zhao, L. Lin, Q. Zhou, Y. Li, S. Yuan, Q. Chen, S. Dong, and J. Wang, Surface vacancy-induced switchable electric polarization and enhanced ferromagnetism in monolayer metal trihalides, *Nano Lett.* **18**, 2943 (2018).
- [42] D. Di Sante, A. Stroppa, P. Barone, M.-H. Whangbo, and S. Picozzi, Emergence of ferroelectricity and spin-valley properties in two-dimensional honeycomb binary compounds, *Phys. Rev. B* **91**, 161401(R) (2015).
- [43] J. Zhang, T. Altalhi, and B. I. Yakobson, Flexo-ferroelectricity and a work cycle of a two-dimensional-monolayer actuator, *ACS Nano* **17**, 5121 (2023).
- [44] R. A. Cowley, Structural phase transitions I. Landau theory, *Adv. Phys.* **29**, 1 (1980).
- [45] R. X. Fei, W. Kang, and L. Yang, Ferroelectricity and phase transitions in monolayer group-IV monochalcogenides, *Phys. Rev. Lett.* **117**, 097601 (2016).
- [46] L. Li, Y. Xia, M. Zhao, C. Song, J. Li, and X. Liu, The electronic structure of a single-walled aluminosilicate nanotube, *Nanotechnology* **19**, 175702 (2008).
- [47] M. Zhao, Y. Xia, and L. Mei, Energetic minimum structures of imogolite nanotubes: A first-principles prediction, *J. Phys. Chem. C* **113**, 14834 (2009).
- [48] L. Z. Zhang, F. Zhai, K. H. Jin, B. Cui, B. Huang, Z. Wang, J. Lu, and F. Liu, Quantum spin Hall effect and tunable spin transport in As-graphane, *Nano Lett.* **17**, 4359 (2017).
- [49] L. Wang, K. Cai, J. Shi, and Q. Qin, Self-assembly of nano-scroll/nano-helix from a diamondene nanoribbon with one passivated surface, *Appl. Surf. Sci.* **527**, 146848 (2020).